Transport and Communications Science Journal

NUMERICAL ANALYSIS AND COMPARISON OF DOWEL LOAD TRANSFER MODELS IN JOINTED PLAIN CONCRETE PAVEMENTS USING THE FINITE ELEMENT METHOD

Hoang Khac Tuan[1*], Pham Ngoc Thach[2]

[1]Boydens Vietnam part of Sweco, No 235 Nguyen Van Cu Street, Cau Ong Lanh Ward, Ho Chi Minh City, Vietnam

[2]Ho Chi Minh City University of Transport, No 2 Vo Oanh Street, Thanh My Tay Ward, Ho Chi Minh City, Vietnam

ARTICLE INFO

TYPE: Research Article
Received: 02/08/2025
Revised: 27/09/2025
Accepted: 12/01/2026
Published online: 15/01/2026
https://doi.org/10.47869/tcsj.77.1.8

[*] *Corresponding author*
Email: tuan.hoang@sweco.vn; Tel: +84 898898842

Abstract. Jointed Plain Concrete Pavements (JPCPs) are divided by transverse and longitudinal joints, with dowel bars commonly embedded across transverse joints to ensure adequate load transfer efficiency (LTE) between adjacent slabs. However, joints are often considered the primary source of long-term structural deterioration. Thus, accurate modeling of joint behavior is essential for comprehensive analysis of the structural response of JPCPs systems. This study investigates LTE performance using three-dimensional finite element models developed in ABAQUS, employing three dowel–concrete interaction approaches: (1) surface contact with Coulomb friction; (2) embedded constraint method; and (3) spring connection. All three models produced consistent LTE values and closely matched field measurements. However, notable differences were identified in terms of modeling complexity, mesh density, numerical stability, and the ability to capture local stress around the dowel bars. These distinctions underscore the importance of aligning the modeling approach with the specific objectives of the analysis. The frictional contact model allows for detailed stress evaluation at the dowel–concrete interface but requires greater computational resources and modeling effort. In contrast, the embedded constraint and spring connection methods are better suited for large-scale simulations that focus on overall slab deformation, where local stress analysis at the dowel interface is not required.

Keywords: jointed plain concrete pavements, dowel bar, load transfer efficiency, finite element method, ABAQUS.

1. INTRODUCTION

Jointed Plain Concrete Pavements consist of individual concrete slabs connected by steel bars at longitudinal and transverse joints. Tie bars are typically placed at longitudinal joints to maintain slab alignment. At transverse joints, larger and more closely spaced dowel bars are embedded to transfer loads between adjacent slabs. Under wheel loading, a portion of the stress is transmitted through the dowels, which reduces localized deflection and improves pavement durability. The effectiveness of this load-sharing mechanism is quantified by the load transfer efficiency, defined as the ratio of deflection in the unloaded slab to that in the loaded slab [1].

$$LTE = \left(\frac{d_u}{d_l} \right) \; x \; 100\% \tag{1}$$

Where:

d_u = the corresponding deflection at the joint of the unloaded slab.

d_l = the maximum deflection at the joint of the loaded slab.

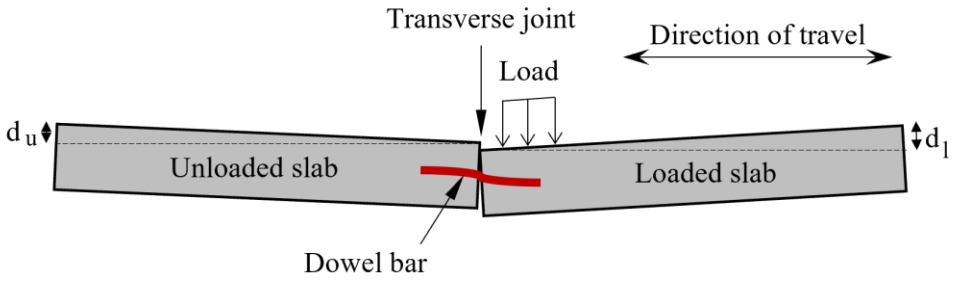

Figure 1. Load transfer mechanism across a transverse joint using dowel bars.

Load transfer efficiency is commonly evaluated in the field using the falling weight deflectometertest, which measures relative vertical displacement between adjacent slabs under loading conditions [2,3]. To complement experimental testing, three-dimensional finite element modeling has been extensively employed to simulate load transfer at transverse joints and to estimate LTE values [3-5]. The finite element modeling approach offers detailed representation of pavement components, including slabs, dowels, base layers, and subgrade, as well as their mechanical interactions. This study investigates three dowel–concrete interaction models: (1) surface contact with Coulomb friction (Model M1), which explicitly simulates interface behavior and allows realistic representation of frictional interaction between the dowel surface and surrounding concrete; (2) the embedded constraint method (Model M2), which simplifies the interaction by constraining translational degrees of freedom [6,7]; and (3) the spring connection model (Model M3), which employs zero-length springs to represent axial and shear resistance along the dowel bars [8-10].

The objective of this study is to evaluate and compare the performance of these modeling approaches under falling weight deflectometerloading. The models are validated against experimental data, and their accuracy, computational efficiency, numerical stability, and suitability for parametric analysis are assessed. The findings aim to guide model selection in future JPCPs analyses and large-scale pavement design.

2. FINITE ELEMENT MODELING

2.1. Simulation details of model M1

The falling weight deflectometer test is simulated in the model as a static, uniformly distributed pressure applied over a circular area [2,3]. The pavement structure included two concrete slabs over a cement-stabilized subbase, a frost protection layer, and a subgrade. To reduce computational time, slab length was shortened from 4.50 m to 2.25 m. This reduction does not significantly affect local stress and deformation near dowels. Fourteen steel dowel bars, 30 mm in diameter and 500 mm in length, were embedded at mid-slab with 0.23 m spacing. A static pressure of 0.70 MPa was applied over a 0.32 m diameter area, located 0.09 m from the transverse joint. All materials were modeled as linear elastic, with properties based on field tests (Table 1).

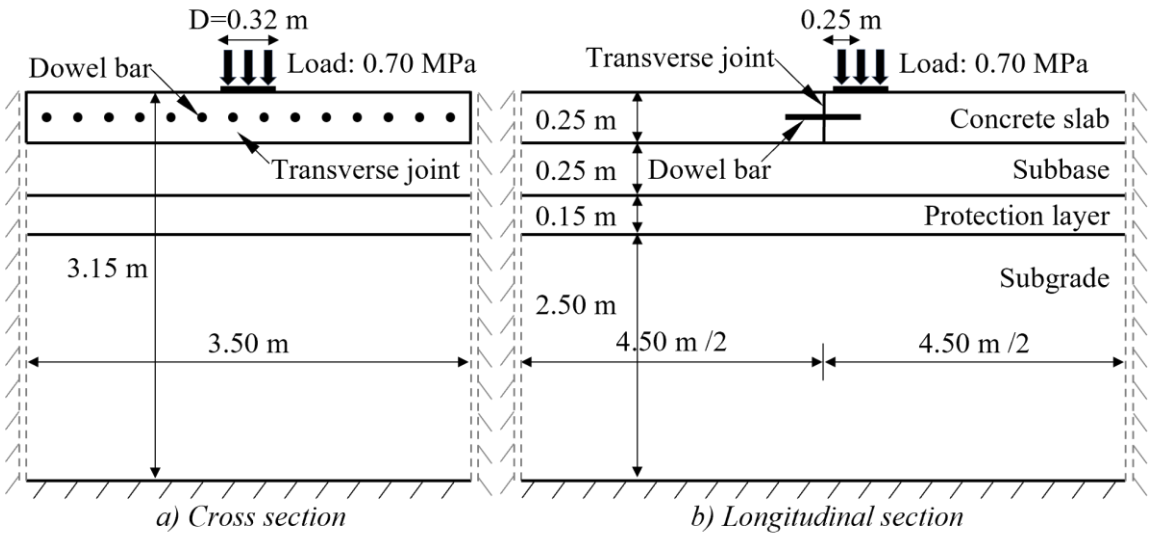

Figure 2. Experimental pavement configuration by Piotr Mackiewicz [3].

Table 1. Material properties and layer thicknesses used in the finite element model.

Number	Materials	Parameters	Values	Thickness
1	Concrete slab	Modulus of elasticity Poisson's ratio	35000 MPa 0.20	0.25 m
2	Subbase (cement-stabilized aggregate)	Modulus of elasticity Poisson's ratio	2900 MPa 0.30	0.25 m
3	Frost-protection (crushed stones)	Modulus of elasticity Poisson's ratio	193 MPa 0.35	0.15 m
4	Subgrade	Modulus of elasticity Poisson's ratio	143 MPa 0.35	2.50 m
5	Steel dowel bar	Modulus of elasticity Poisson's ratio	210000 MPa 0.30	—

The finite element model consisted of the concrete slab, subbase, protection layer, subgrade, and dowel bars. All pavement layers and dowel bars were discretized using 8-node linear continuum three-dimensional elements (C3D8). These elements, which possess three translational degrees of freedom per node, were selected to accurately capture local stress concentrations and strain around dowel bars due to their full integration scheme, which avoids hourglass modes and enhances stress resolution.The full model comprised approximately

271330 elements, ensuring sufficient resolution for reliable results. Contact behavior was defined using Coulomb friction in the tangential direction and hard contact in the normal direction to allow separation between surfaces [12]. According to [11], the friction coefficient between the slab and base ranges from 0.90 to 2.20, depending on the base type. A value of 1.80 was selected to represent the cement-stabilized subbase. The same contact definition was applied at the interfaces between the subbase and protection layer, and between the protection layer and subgrade. Interaction between the slab and dowel bars was modeled using surface-to-surface contact. Coulomb friction with a coefficient of 0.30 was applied on the bonded side of the dowel, while a reduced friction coefficient of 0.05 was assigned to the free side to reflect partial restraint [4]. The interaction between foundation layers also needs to be defined [4,13]. The friction coefficients between the subbase and the frost-protection layer, as well as between the frost-protection layer and the subgrade, were specified as 1.0, following the value reported in [13]. Friction at the transverse joint was neglected to reflect realistic conditions, where joint sealant prevents direct contact and allows slab movement due to thermal and moisture effects [11].

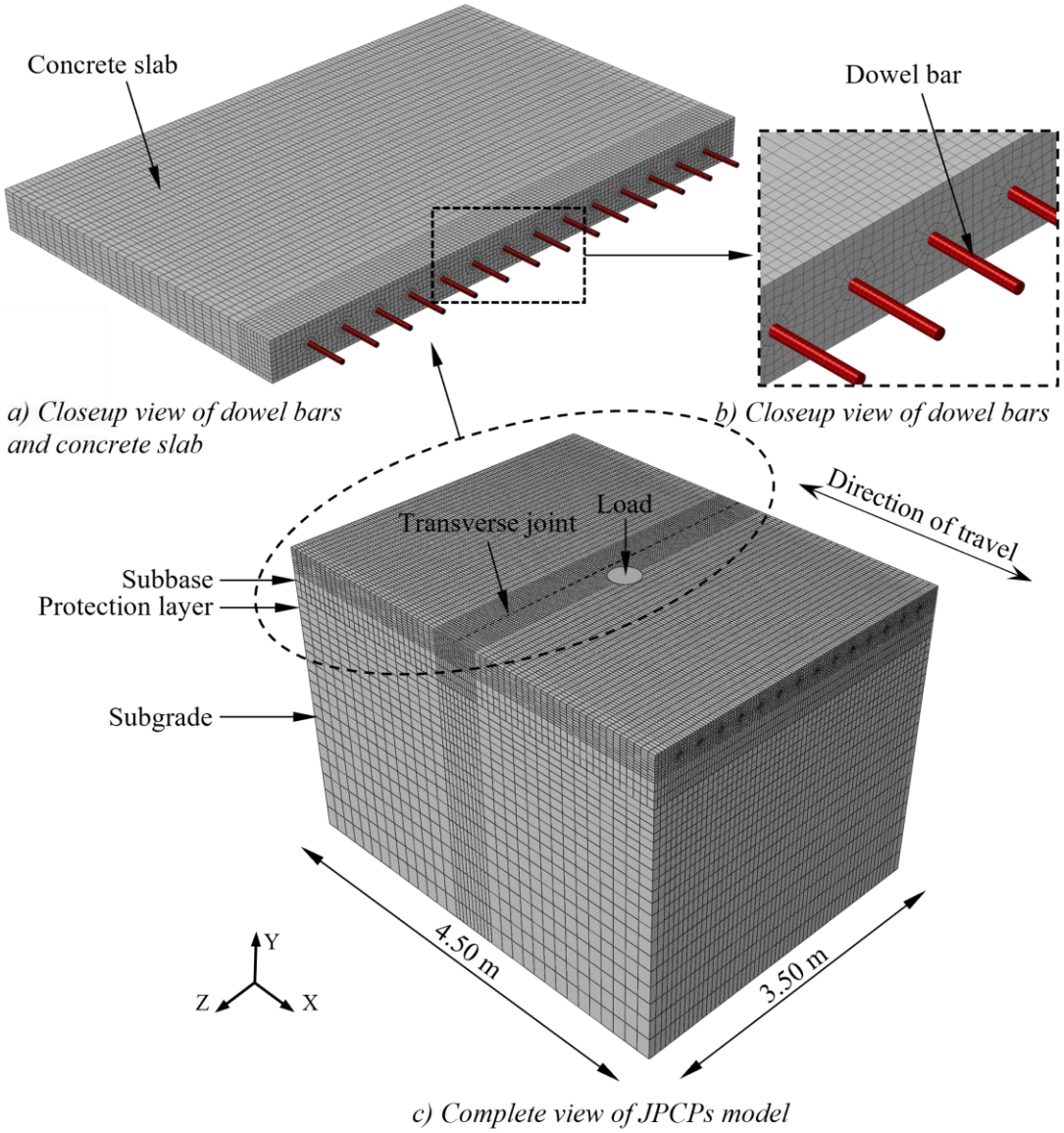

Figure 3. Three-dimensional finite element modeling of JPCPs.

Symmetry was applied along vertical faces perpendicular to the longitudinal axis (x-direction), restricting displacement in x ($U_x = 0$). Vertical faces along the transverse axis (z-direction) were constrained in z ($U_z = 0$) to simulate the restraint from adjacent slabs. A subgrade thickness of 2.50 m was selected based on a convergence study, as increasing the thickness beyond this value caused negligible changes in the results, consistent with the findings in [3,4,5]. The bottom surface of the subgrade was fully fixed in all directions ($U_x = U_y = U_z = 0$), representing a rigid, bonded subgrade foundation.

2.2. Simulation details of model M2

Figure 4 illustrates the finite element modeling configuration for simulating dowel–concrete interaction in JPCPs. The concrete slab and subbase were modeled using C3D8 solid elements, while dowel bars were represented by B31 beam elements. Each B31 element consists of two nodes, with each node possessing three translational and three rotational degrees of freedom, resulting in 12 degrees of freedom per element. The concrete domain serves as the host region in the embedded method, with a total of approximately 93276 finite elements used in the model.

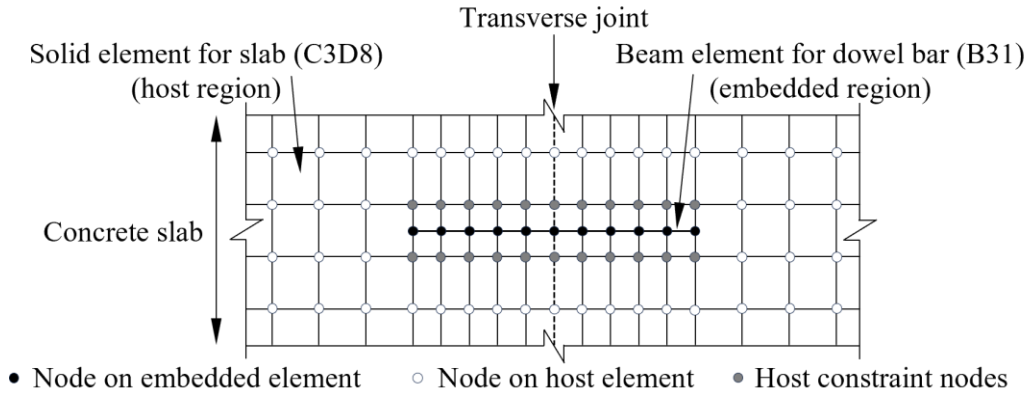

Figure 4. Embedded constraint scheme.

The interaction between dowel bars and concrete was simulated using the embedded constraint method. In this approach, the translational degrees of freedom of the embedded beam nodes are fully constrained through interpolation from surrounding host solid elements [6,7,8], ensuring displacement compatibility and enabling effective transfer of axial and shear forces. The rotational degrees of freedom remain unconstrained [8], allowing realistic bending behavior of the dowel bars. Despite the embedding, the stiffness of the beam elements is retained in the global stiffness matrix, contributing to the overall structural response.

2.3. Simulation details of model M3

In model M3, the dowel bars were modeled using linear B31 beam elements and the concrete slabs using C3D8 solid elements, consistent with the element types employed in model M2. However, the main difference is the modeling approach for the dowel–concrete interaction. Each spring element was oriented along the local axis connecting the coincident nodes of the beam and solid elements. The mechanical linkage between the two domains was simulated using linear elastic zero-length spring elements, providing resistance to axial separation, compression, or slip. The stiffness of the springs was defined based on a modulus of dowel support of $k = 407.3 \times 10^6$ kN/m³, as reported in experimental studies [14,15]. The

model comprised approximately 82472 elements. The equivalent discrete spring stiffness is determined by equation (2):

$$Ks = K \cdot D \cdot L \tag{2}$$

Where Ks is the equivalent discrete spring stiffness (kN/m), K is the modulus of dowel support (kN/m³), D is the dowel bar diameter (m), L is the spacing between two adjacent spring nodes (m).

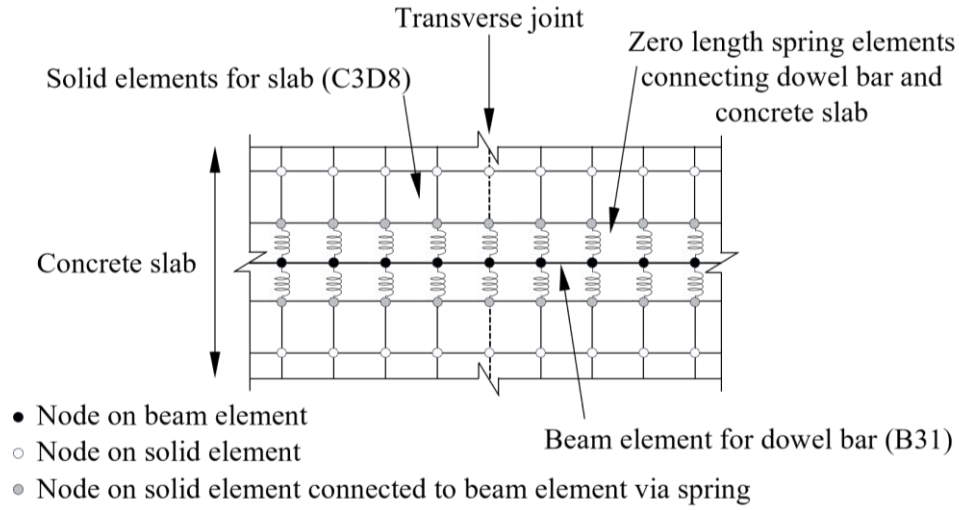

Figure 5. Zero-length spring connection scheme.

Figure 5 illustrates the zero-length spring connection scheme in detail. Table 2 summarizes the primary modeling characteristics of the finite element modeling models developed for JPCPs. Although all models share identical pavement geometry and layer discretization, they differ notably in the representation of element type, total number of elements, mesh density, dowel–concrete interaction, modeling effort, and computational efficiency.

Table 2. Summary of modeling characteristics of the three-dimensional finite element modeling.

Criteria	Model M1	Model M2	Model M3
Pavement layer element type	C3D8	C3D8	C3D8
Dowel bar element type	C3D8	B31	B31
Total number of elements	271330	93276	82472
Mesh density	High – fine mesh required around dowel–slab interface	Moderate – standard mesh density	Moderate – require extra setup for spring connections
Dowel–concrete Interaction	Surface-to-surface contact with Coulomb friction	Embedded method constraining translational DOFs	Axial and shear resistance via zero-length spring elements
Modeling effort	High – complex contact and mesh compatibility	Low – straightforward implementation using built-in constraints	High – requires definition of spring stiffness and coincident node alignment

3. RESULTS AND DISCUSSION

3.1. Analysis of vertical displacement in finite element modeling

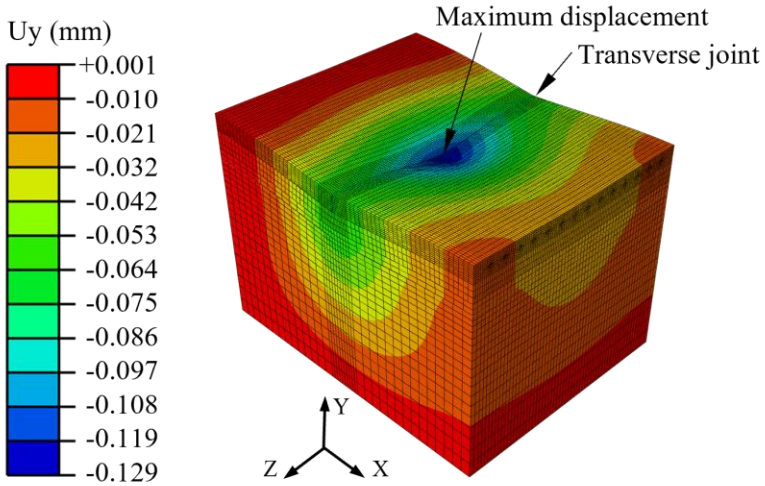

a) Color contour plot of vertical displacement (Uy) in model M1.

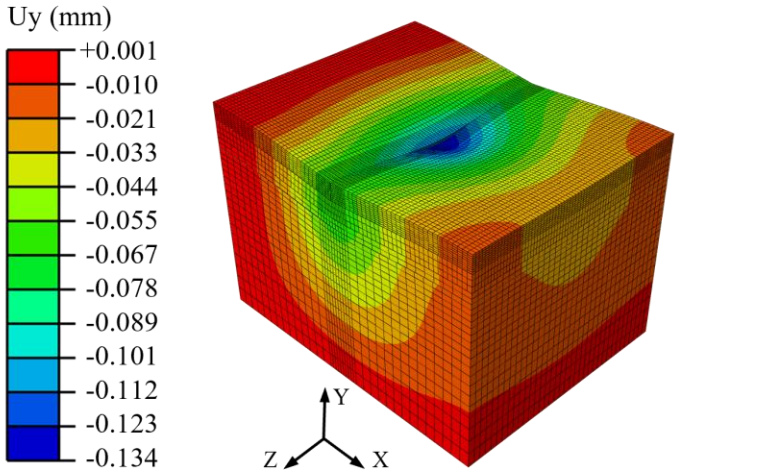

b) Color contour plot of vertical displacement (Uy) in model M2.

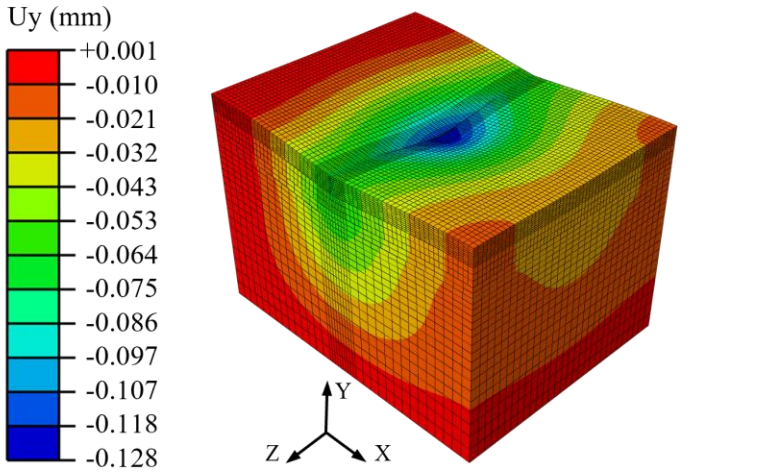

c) Color contour plot of vertical displacement (Uy) in model M3.

Figure 6. Color contour plot of vertical displacement (Uy).

The contour plots in Figure 6 illustrate the vertical displacement (U_y) distribution in model M1, M2 and M3 under static loading conditions. All models exhibit similar deformation patterns, with the maximum vertical deflection consistently observed at the transverse joint between the loaded and unloaded concrete slabs. Notably, the peak displacement occurs on the edge of the loaded slab, leading to a measurable deflection differential between the two slabs. This behavior indicates that the LTE is less than 100%, which is consistent with field observation, as LTE is strongly influenced by the joint design and configuration of the dowel bar system. Due to the presence of the dowel bar system, the variation in U_y displacement on either side of the loading point along the transverse direction (z-axis) is significantly smaller than that along the longitudinal direction (x-axis) of the two slabs.

Figure 7 presents the vertical displacement (U_y) responses of the loaded slab for Models M1, M2, and M3 across the transverse joint under loading conditions. All three models exhibit similar deformation patterns, with symmetrical vertical displacements distributed across the transverse joint. The peak vertical displacements occur near the center of the slab, consistent with the location of the applied load. Among the three models, M2 exhibited the largest deflection (−0.134 mm), followed by M1 (−0.129 mm) and M3 (−0.128 mm). The difference in peak deflection between M2 and the other two models is approximately 3.9% compared to M1 and 4.7% compared to M3. These values indicate that M1 and M3 achieved more effective load transfer across the transverse joint than M2, as evidenced by their lower deflections under the same loading conditions. The nearly identical deflection values of M1 and M3 suggest comparable structural performance in terms of LTE, despite differences in modeling approach and complexity.

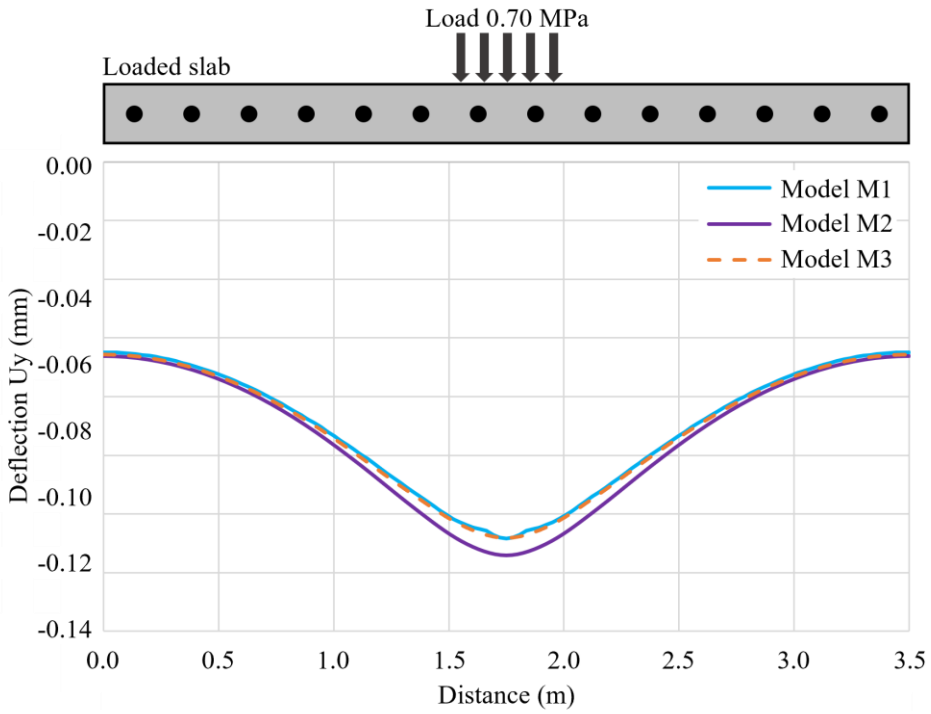

Figure 7. Comparison of deflection responses for the loaded slab at transverse joint.

Figure 8 illustrates the vertical displacement (U_y) profiles of the unloaded slab for Models M1, M2, and M3 across the transverse joint. All three models exhibit similar deformation patterns, with symmetrical vertical displacements along the slab. These deflections represent the structural response of the unloaded slab under load transmitted via dowel bars from the adjacent loaded slab. Among the models, M2 displays the largest deflection of −0.116 mm, whereas M1 and M3 show smaller values of −0.112 mm. The slightly smaller deflections in M1 and M3, approximately 3.6% lower than M2, indicate more effective load transfer, consistent with their higher LTE values and reduced deflections in the loaded slab. These findings confirm that M1 and M3 provide better joint performance by minimizing differential movement between adjacent slabs.

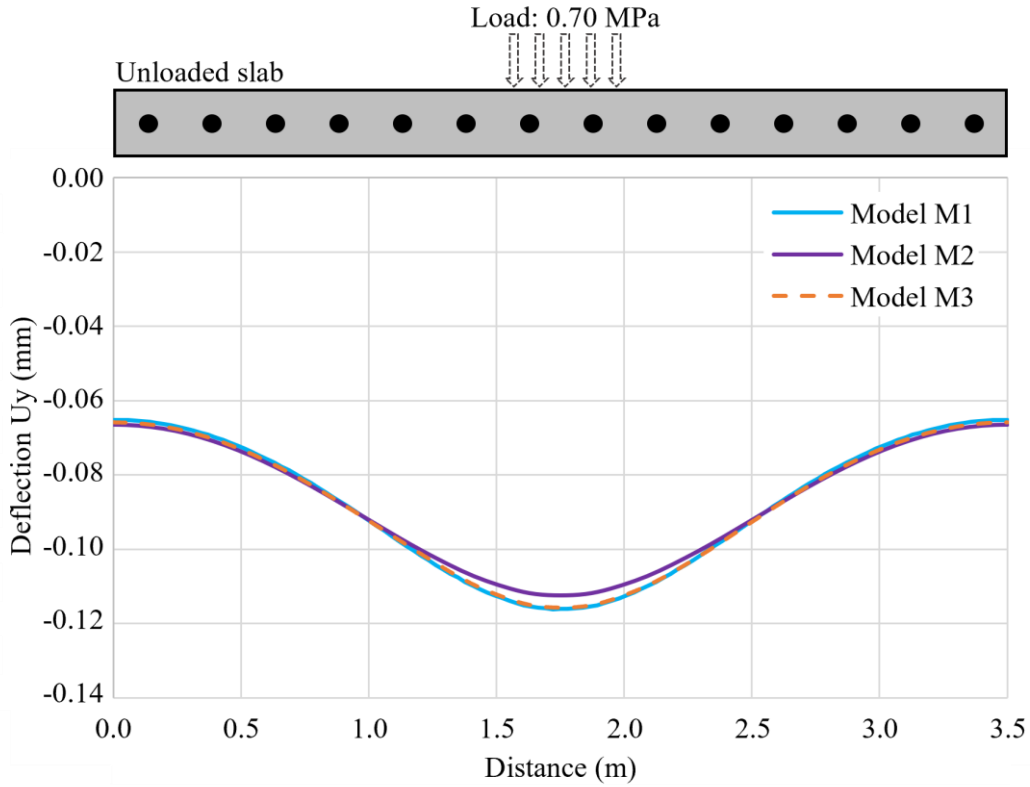

Figure 8. Comparison of deflection responses for the unloaded slab at the transverse joint.

3.2. Comparison of the finite element modeling with falling weight deflectometer test

Figure 9 compares the simulated vertical deflection profiles of Models M1, M2, and M3 with field measurements from an falling weight deflectometer test [3] across a transverse joint. The deflection curves of all three models demonstrate good agreement with the experimental data, particularly in the vicinity of the peak deflection. The maximum vertical displacements (Uy) observed at the loaded slab for Models M1, M2, and M3 were −0.129 mm, −0.134 mm, and −0.128 mm, respectively, while the corresponding deflections at the unloaded slab were −0.116 mm, −0.112 mm, and −0.116 mm. These values result in calculated LTEs of 89.9%, 83.6%, and 90.6% for Models M1, M2, and M3, respectively. These results are consistent with expected field performance, where LTE is typically less than 100% due to imperfect load transfer across transverse joints. The minor differences among

models reflect the influence of different dowel modeling techniques on joint behavior. All three models showed similar load transfer behavior, with LTE values consistent with field data. M1 and M3 performed slightly better than M2, as indicated by smaller deflection differences between the slabs.

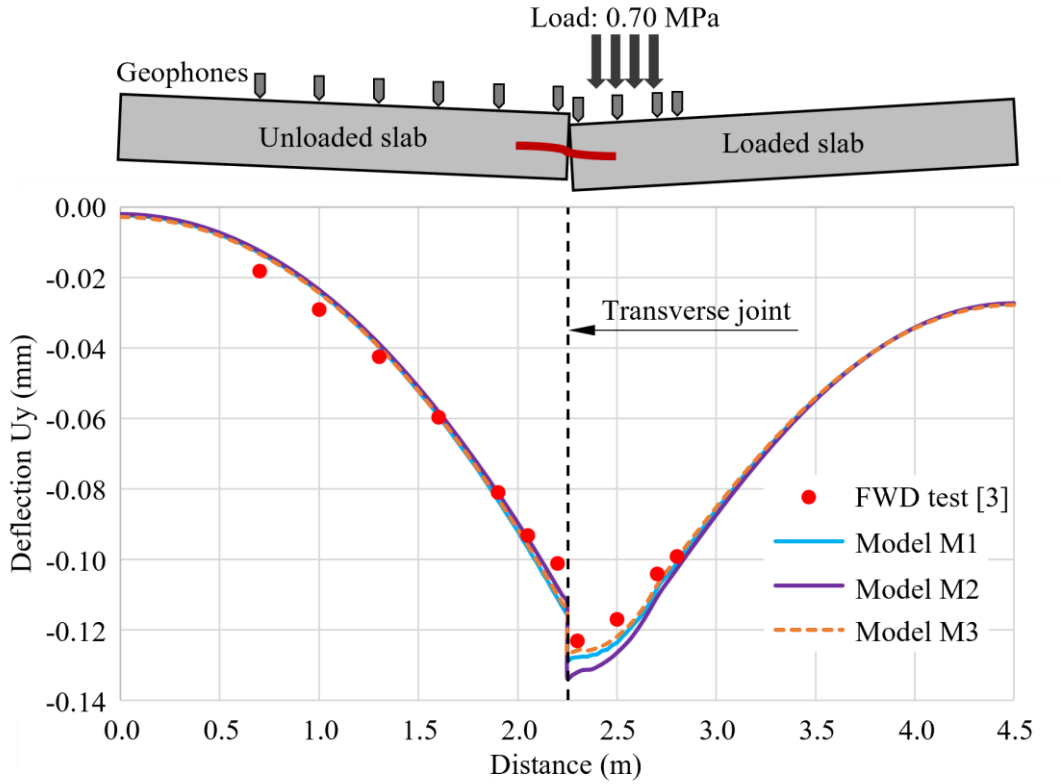

Figure 9. Comparison of experimental results with three-dimensional finite element modeling.

3.3. Comparison of M1, M2 and M3 modeling techniques

Table 3 presents a comparative summary of the numerical performance and modeling capabilities of the three finite element approaches. The models are evaluated based on key metrics such as vertical deflection, load transfer efficiency, stress output capabilities, computational demand, and their applicability for further parametric investigations.

In summary, while all three finite element models demonstrate comparable load transfer performance, their distinct modeling strategies lead to different balances among computational efficiency, numerical stability, and stress output capabilities. These differences should be carefully considered when selecting an appropriate modeling approach for specific research objectives. In particular, Models M2 and M3 may offer practical advantages for large-scale or parametric studies due to their stable performance and reduced computational demands, especially when detailed stress analysis at the dowel–concrete interface is not required. On the other hand, Model M1 is more suitable for investigations that require explicit simulation of contact interactions and detailed stress distribution around dowel bars and within the surrounding concrete at dowel holes.

Table 3. Summary of modeling characteristics of the three-dimensional finite element modeling.

Criteria	Model M1	Model M2	Model M3
Maximum Uy (loaded slab)	-0.129 mm	-0.134 mm	-0.128 mm
Maximum Uy (unloaded slab)	-0.116 mm	-0.112 mm	-0.116 mm
Estimated LTE	89.9%	83.6%	90.6%
Loaded transfer performance	Good – consistent with field results	Good – slightly lower than M1 and M3	Good – consistent with field results
Stress output at dowel–concrete interface	Available – allows evaluation of local stress concentration near dowels	Not available – embedded method does not allow stress output at interface	Not available – springs do not support stress output
Numerical stability	Sensitive – contact convergence issues possible	Stable	Stable
Computational time	*T* - long, attributed to dense mesh and computationally demanding 3D contact modeling	0.13*T* - short, resulting from simplified embedded constraints	0.30*T* - moderate, reflecting fewer elements but additional spring-based linkage formulation
Suitability for parametric study	Moderate – requires remeshing for geometry/contact changes	High	High

Note. T represents the computation time of Model M1 and serves as the reference baseline.

4. CONCLUSION

This study evaluated three finite element modeling approaches for simulating dowel–concrete interaction in JPCP systems: surface contact with Coulomb friction (Model M1), embedded constraint method (Model M2), and spring connection (Model M3). All models reproduced realistic load transfer behavior, with consistent LTE values and deflection patterns that align well with field measurements, confirming their reliability for structural analysis of transverse joints.

Each model has its own advantages and limitations. Model M1 enables local stress evaluation at the dowel–concrete interface and achieves high load transfer accuracy, but it requires dense mesh, complex contact definitions, and significantly longer computation time. Model M2 is the most computationally efficient and numerically stable, while Model M3 provides a simplified linkage scheme with good balance between modeling effort and performance, though both do not support stress output at the dowel–concrete interface.

All three models demonstrated good load transfer performance. However, Models M2 and M3 are especially well-suited for large-scale simulations focused on global stress and deformation of concrete slabs, where localized stress evaluation around dowel bars is not essential.

Overall, the findings provide practical guidance for pavement engineers in selecting the most appropriate finite element modeling approach based on project scale, computational resources, and required output detail. The study emphasizes the need to balance modeling

accuracy and computational efficiency when analyzing load transfer in jointed plain concrete pavements.

REFERENCES

[1]. Federal Highway Administration (FHWA), Pavement Performance Measures and Forecasting and the Effects of Maintenance and Rehabilitation Strategy on Treatment Effectiveness (Revised), FHWA-HRT-17-095, McLean, VA, USA, 2017.
[2]. H. B. Muslim, S. W. Haider, Effects of seasonal and diurnal falling weight deflectometer measurements on LTE of JPCP—LTPP SMP Data, Federal Highway Administration, Report No. FHWA-HRT-22-094, VA, USA, 2022.
[3]. P. Mackiewicz, Finite-element analysis of stress concentration around dowel bars in jointed plain concrete pavement, Journal of Transportation Engineering, 141 (2015) 06015001. https://doi.org/10.1061/(ASCE)TE.1943-5436.0000768
[4]. A.E. Abu El-Maaty, G.M. Hekal, E.M.S. El-Din, Modeling of dowel jointed rigid airfield pavement under thermal gradients and dynamic loads, Civil Engineering Journal, 2 (2016) 38–51. https://doi.org/10.28991/cej-2016-00000011
[5]. A. Jagadeesh, W. A. A. S. Premarathna, A. Kumar, C. Kasbergen, S. Erkens, Finite element modelling of jointed plain concrete pavements under rolling forklift tire, Engineering Structures, 328 (2025) 119705. https://doi.org/10.1016/j.engstruct.2025.119705
[6]. H. Dejene, M. Bogale, M. Rynkovskaya, Numerical analysis of the shear behavior of shallow-wide concrete beams via the concrete damage plasticity model, Civil Engineering Journal, 11 (2025) 779–797. https://doi.org/10.28991/CEJ-2025-011-02-022
[7]. Soltanpour, Sina, Sheikhi, Morteza, Numerical and Finite Element Analysis of RC Beams Strengthened With a Novel Technique Using External Plates and Rebars, Advances in Civil Engineering, 1 (2025) 8815587. https://doi.org/10.1155/adce/8815587
[8]. Dassault Systèmes, ABAQUS 6.14 theory manuals, Providence, RI, USA, 2014.
[9]. S.R. Maitra, K.S. Reddy, L.S. Ramachandra, Load transfer characteristics of dowel bar system in jointed concrete pavement, Journal of Transportation Engineering, 135 (2009) 813–821. https://doi.org/10.1061/ASCETE.1943-5436.0000065
[10]. W.G. Davids, Z. Wang, G. Turkiyyah, J.P. Mahoney, D. Bush, Three-dimensional finite element analysis of jointed plain concrete pavement with EverFE2.2, Transportation Research Record, 1853 (2003) 92–99. https://doi.org/10.3141/1853-11
[11]. AASHTO (American Association of State Highway and Transportation Officials), AASHTO Guide for Design of Pavement Structures, Part II: Rigid Pavement Design, Washington, D.C., USA, 1993.
[12]. H.K. Tuan, N.T. Pham, Numerical simulation of concrete pavement response to temperature gradients, Journal of Transportation Science and Technology, 11 (2020) 24–33. (In Vietnamese). https://doi.org/10.55228/JTST.11(2).24-33
[13]. S. Yaqoob, J. Silfwerbrand, R.G.R. Balieu, A Parametric Study Investigating the Dowel Bar Load Transfer Efficiency in Jointed Plain Concrete Pavement Using a Finite Element Model, Buildings, 14 (2024) 1039. https://doi.org/10.3390/buildings14041039
[14]. H. Guo, J.A. Sherwood, M.B. Snyder, Component dowel bar model for load transfer systems in PCC pavements, Journal of Transportation Engineering, 121 (1995) 289–298. https://doi.org/10.1061/(ASCE)0733-947X(1995)121:3(289)
[15]. K. Bhattacharya, Nonlinear Response of Transverse Joints of Airfield Pavements, Journal of Transportation Engineering, 126 (2000) 168–177. https://doi.org/10.1061/(ASCE)0733-947X(2000)126:2(168)